Journal of Building Engineering 103 (2025) 112205

Contents lists available at ScienceDirect

Journal of Building Engineering

journal homepage: www.elsevier.com/locate/jobe

Rotating semi-active tuned liquid column damper for bi-directional eccentric structural seismic response control

Cong Fu [a], Liangkun Wang [a,*], Zhipeng Wang [b], Songtao Xue [a], Liyu Xie [a]

[a] Department of Disaster Mitigation for Structures, Tongji University, Shanghai, 200092, China
[b] Department of Control Science and Engineering, Tongji University, Shanghai, 201804, China

ARTICLE INFO

Keywords:
Tuned liquid column damper
Semi-active control
Eccentric structure
Translational-torsional coupling control
Variable angle
Semi-active damping

ABSTRACT

To mitigate the translational-torsional coupling response of bi-directional eccentric buildings under seismic excitations and improve the earthquake mitigation of traditional tuned liquid column damper (TLCD), a rotating semi-active TLCD (RS-TLCD) with variable hydrostatic liquid level height and frequency, damping and rotating angle that can simultaneously control the bi-directional vibration of structures is proposed. RS-TLCD can identify the bi-directional instantaneous vibration frequency of structure through wavelet transform, and change the height of liquid column in real time to adjust its natural frequency accordingly. Meanwhile, it can change the size of adjustable flow hole to achieve real-time semi-active damping based on measured signals, while use a rotating chassis to achieve real-time adjustment of the position angle in the plane to the dominant vibration direction, to achieve bi-directional vibration control. In the case study, a 30-story bi-directional eccentric structure is presented to verify its seismic control effect, and cases with unidirectional passive TLCDs and S-TLCDs attached in X and Y directions are compared respectively. Numerical results show that generally, RS-TLCD can effectively control the displacement and torsional response of building under earthquake excitations to improve its safety and has the best earthquake mitigation performance in both X and Y directions. Meanwhile, RS-TLCD can reduce the mass of damper and the occupation of the building space because it can rotate the position angle to the dominant vibration direction, and enhance the control effect through variable liquid level height and damping.

1. Introduction

For eccentric building structures with the misalignment between the mass center and stiffness center due to functional requirements and other factors, they will simultaneously exhibit both translational and torsional responses within the horizontal plane under seismic excitations, which significantly impact on the structural safety. Therefore, it is essential to reduce the translational-torsional coupling vibration of the structure under earthquake excitations.

Structural vibration control is a commonly used method in energy dissipation and earthquake mitigation, such as tuned mass damper and inerter damper [1,2], which have a wide range of applications in practical engineering. Among it, tuned liquid damper (TLD) is a traditional dynamic absorber that utilizes the dynamic side force generated during the oscillation of liquid in fixed water tank to provide vibration mitigation. Therefore, it is also named the tuned sloshing damper. The structural characteristic of TLD is that

* Corresponding author.
E-mail address: wangliangkun@tongji.edu.cn (L. Wang).

https://doi.org/10.1016/j.jobe.2025.112205
Received 22 December 2024; Received in revised form 16 February 2025; Accepted 22 February 2025
Available online 25 February 2025

the liquid inside tank participates in the sloshing. However, its frequency and damping are difficult to be adjusted, which limits its structural vibration mitigation. Tuned liquid column damper (TLCD), a derivative of TLD, is a cost-effective, easily installed, frequency adjustable and simple to maintain device for structural control. During its operational process, a U-shaped constant cross-section tubular rigid tank with its lower part fixed to the structure allows for structural vibration to be transferred to TLCD, causing the internal water to move back and forth. This movement of water obtains damping force through viscous interaction with the container and water head loss caused by passing through water orifices during the back-and-forth motion which dissipates the kinetic energy of structure and reduces its vibration. At the same time, the inertia force generated by the water movement acts in the opposite direction of structural vibration, further reducing the vibration of structure. At this time, expert scholars have optimized the TLCD to achieve improved control effect by various methods including transforming the water in the device into high-viscosity fluids such as water-glycol mixtures [3], altering the external shape and internal roughness of the TLCD [4,5], using interconnected vertical columns or ring containers to control multi-directional vibrations [6,7], replacing orifices with a rolling ball [8,9] and ball coupling spring which can translate as well as rotate [10], installing various devices in the horizontal section of TLCD to change the damping coefficient [11], sealing vertical air column singularly for vertical vibration control by adjusting the stiffness of air spring [12], etc. In addition, many scholars have studied TLCD for dynamic control of offshore structures [13–16].

Nevertheless, the control effect of traditional passive TLCD is sensitive to its own parameters. When the structural natural frequency varies caused by suffering damage, the control effect of passive TLCD will be significantly diminished. Additionally, passive TLCDs have a poor vibration control performance across a wide frequency band of building structure. Therefore, achieving adaptive adjustment of TLCD parameters under seismic excitation to enhance its real-time control performance is crucial. To overcome the limitations of passive control system, researchers have developed the semi-active control system [17,18], known as semi-active TLCD (S-TLCD) [19–23]. S-TLCD can dynamically modify damping or frequency in real-time based on corresponding control algorithm aiming to accommodate different vibration reduction needs at various moments. Both theoretical analysis and experimental studies have shown that this type of control system can further reduce structural vibration better than the passive system. Sonmez et al. [24] proposed a novel S-TLCD which was attached to the primary structure using an adaptive spring, whose stiffness was controlled by short time Fourier transformation-based feedforward and feedback algorithms. Ding et al. [25] proposed an event-triggered semi-active technique which could achieve the rapid activation of TLCDs through baffles to improve the vibration suppression performance of TLCDs in the early stage of structural vibration. Masnata et al. [26] introduced a sliding TLCD which was implemented on a roller support using a spring-dashpot system to connect the base-isolated subsystem. Wang et al. [27] combined magnetorheological (MR) fluid with TLCD to form a semi-active MR-TLCD, using an external magnetic field to control the damping ratio of TLCD in real time. Liu et al. [28] investigated a vertical tuned liquid column gas damper which was able to tune frequency flexibly through variable equivalent linear air spring stiffness for reducing structural vibrations.

All the above studies have only focused on controlling the vibration in a single direction of structures. However, under external excitations, structures will generate vibrations in multiple directions. Many researchers have explored improving the TLCD device or using multiple TLCDs for vibration control of multiple directions. Lee et al. [29] proposed a tuned liquid column and sloshing damper (TLCSD) for bi-directional structural vibration control. Rozas et al. [30] presented a new bi-directional TLCD for controlling the earthquake response of structures which required less liquid than two equivalent TLCDs. Zhang et al. [31] proposed a semi-active toroidal TLCD to control multidirectional response, which could automatically identify changes in structural frequency and then adjust its frequency by adjusting the liquid level. Mehrkian et al. [32] showed an omnidirectional liquid column vibration absorber with multiple liquid columns with different cross-sections which could be set in any directions because of the rotating platform at the bottom. Ding et al. [33] derived an adapted dynamic model which distinguished between liquid oscillation and sloshing in vertical segment for toroidal TLCDs.

The aforementioned references are all focused on the dynamic control of symmetric buildings. For unsymmetrical building structures with the misalignment of the mass center and stiffness center, an in-plane torsional response under external excitations will be caused. There have been numerous studies conducted by expert scholars on the vibration control of eccentric building structures with translational-torsional coupling vibration. Fu [34] proposed a novel torsional tuned liquid column gas damper for the coupled flexural torsional vibration control of torsional buildings. Hochrainer et al. [35] presented a coupled tuned liquid column gas damper to reduce several modes simultaneously. Ross et al. [36] designed three unique TLD systems to mitigate the torsional response of structures. Pandey et al. [37] integrated tuned liquid column ball damper with circular liquid column ball damper for the torsional coupled vibration control of buildings under wind excitations. Most of these studies utilize multiple dampers for the structural translational-torsional coupling control, which will significantly occupy the structural useable space and affect the functional use of the structure.

To control the translational-torsional coupling vibration simultaneously, improve the utilization efficiency of absorbers, reduce the occupation of building space and influence to the structural normal use, it is meaningful to develop an integrated semi-active controller which can control both translational and torsional responses bi-directionally. To fill this gap, a rotating S-TLCD (RS-TLCD) is proposed in this study. It was experimentally verified in Ref. [38] that changing the height of liquid in the upper water tank of adaptive tuned mass damper could retune its mass and frequency. Inspired by Ref. [38], a function is proposed that the RS-TLCD can dynamically adjust the liquid level height based on comprehensive structural bi-directional vibration signals to regulate its natural frequency in real time. It can also rotate angles in real time to simultaneously control bi-directional vibrations. Furthermore, to enhance the energy dissipation, it can regulate the orifice ratio in real time to achieve real-time adjustment of the nonlinear damping coefficient.

In this paper, the RS-TLCD performs bi-directional translational-torsional coupling control within structural eccentric plane through variable parameters. The control principle and mechanical model of TLCD are introduced in section 2, as well as the electromechanical device and control algorithm of RS-TLCD. Then, equations of motion and a numerical model of a thirty-story bi-directional eccentric building are proposed in section 3. Cases of two optimal X and Y directional passive TLCDs and two unidirectional S-TLCDs with variable liquid level height and damping are presented respectively for comparison. Numerical results are presented and analyzed in section 4. Conclusions are shown in section 5.

2. Electromechanical device and control algorithm of RS-TLCD

2.1. Control principle and mechanical model of TLCD

TLCD dissipates the vibrational energy and controls vibration through viscous interactions between liquid column and container and head losses generated when liquid flows through orifices. Simplified structural diagram with an attached TLCD under earthquake excitation is presented in Fig. 1 [39].

In Fig. 1, orifices are installed in the horizontal segment of TLCD to provide additional damping for TLCD. m_n is the mass of the nth layer of the structure, k_n denotes the stiffness coefficient of the nth layer and $\ddot{x}_g$ represents the earthquake excitation, $\ddot{x}_n$ represents the horizontal acceleration of the layer where TLCD is placed. As for the TLCD system, A_v and A_h are cross-sectional areas of vertical segment and horizontal segment respectively, B means the center-to-center distance between two vertical tubes and H_v represents the hydrostatic liquid level heights in the vertical segment. L is the effective length of the TLCD.

Assuming that the TLCD sway direction is consistent with the direction of TLCD horizontal tube segment, D is the liquid displacement in the vertical tube segment away from the equilibrium position, then the absolute acceleration of liquid in the direction of motion $\ddot{D}$ and the absolute liquid acceleration in the horizontal segment of TLCD in the direction of motion $\ddot{D} + \ddot{x}_n$ can be obtained. As a result, the total inertial force of liquid F_m can be expressed as:

$$F_m = -\left[\rho A_v B\left(\frac{A_v}{A_h}\ddot{D} + \ddot{x}_n\right) + 2\rho H_v A_v \ddot{D}\right] \tag{1}$$

where ρ is liquid density.

The restoring force generated by the deviation from the equilibrium position of TLCD F_R can be written as:

$$F_R = 2\rho A_v g D \tag{2}$$

where g is gravity acceleration.

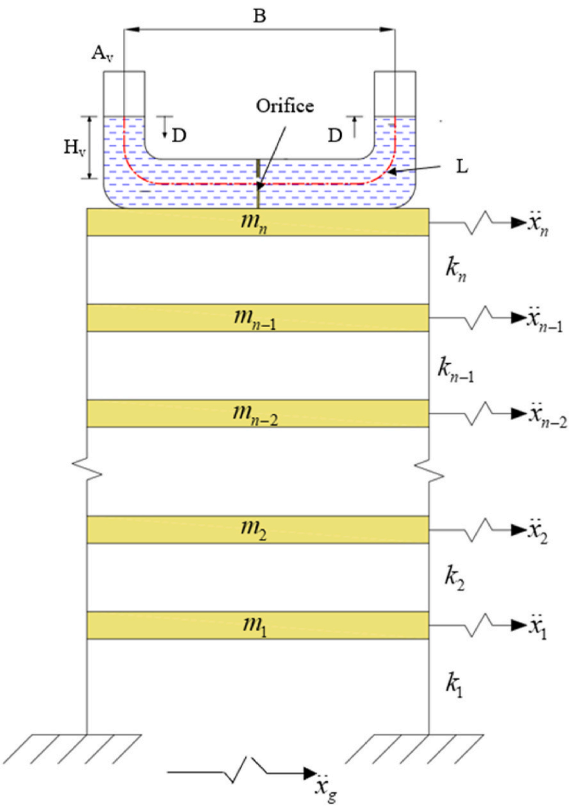

Fig. 1. Typical structural calculation diagram with TLCD under earthquake excitation.

The damping is mainly composed by the frictional resistance along the pipe wall, as well as the damping provided by internal orifices. The friction force F_1 provided by the pipe wall along and the damping force F_2 provided by the internal orifices are considered, which are presented as follows respectively:

$$F_1 = \frac{1}{2}\rho A_h \delta_1 \dot{D}^2 \tag{3}$$

$$F_2 = \frac{1}{2}\rho A_h \delta_2 \lambda^2 \dot{D}^2 \tag{4}$$

where $\dot{D}$ represents the velocity of liquid as it deviates from the equilibrium position in the vertical tube segment, $\lambda = A_v / A_h$ means the area ratio between the vertical segment and horizontal segment of TLCD. In Equation (3), head loss coefficient δ_1 is shown as following:

$$\delta_1 = (1-\lambda)^2 + 0.5|1-\lambda| \tag{5}$$

According to Ref. [40], when liquid flows through a straight pipe with throttle orifice, the head loss coefficient δ_2 is approximated as:

$$\delta_2 = \left[(1-\kappa) + 0.707(1-\kappa)^{0.375}\right]^2 \left(\frac{1}{\kappa}\right)^2 \tag{6}$$

where $\kappa = A/A_h$ is the cross-sectional area ratio of the throttle orifice and horizontal segment of TLCD.

Through Equations (3) and (4), total damping force F can be obtained as:

$$F = F_1 + F_2 = \frac{1}{2}\rho A_h \delta |\dot{D}| \dot{D} \tag{7}$$

where $\delta = \delta_1 + \lambda^2 \delta_2$.

Based on Equation (1)–(7), the motion equation for TLCD is:

$$\left(2\rho A_v H_v + \rho \frac{A_v{}^2}{A_h} B\right)\ddot{D} + \frac{1}{2}\rho \frac{A_v{}^2}{A_h}\delta |\dot{D}|\dot{D} + 2\rho A_v g D = -\rho A_v B \ddot{x}_n \tag{8}$$

From Equation (8), the vibration frequency of TLCD can be derived as:

$$\omega_d = \sqrt{\frac{2\rho A_v g}{2\rho A_v H_v + \rho \frac{A_v{}^2}{A_h} B}} = \sqrt{\frac{2g}{2H_v + \lambda B}} = \sqrt{\frac{2g}{L}} \tag{9}$$

where $L = 2H_v + \lambda B$ represents the effective length of TLCD.

In summary, the vibration frequency of TLCD is depended on its effective length L, and the nonlinear damping force of TLCD system

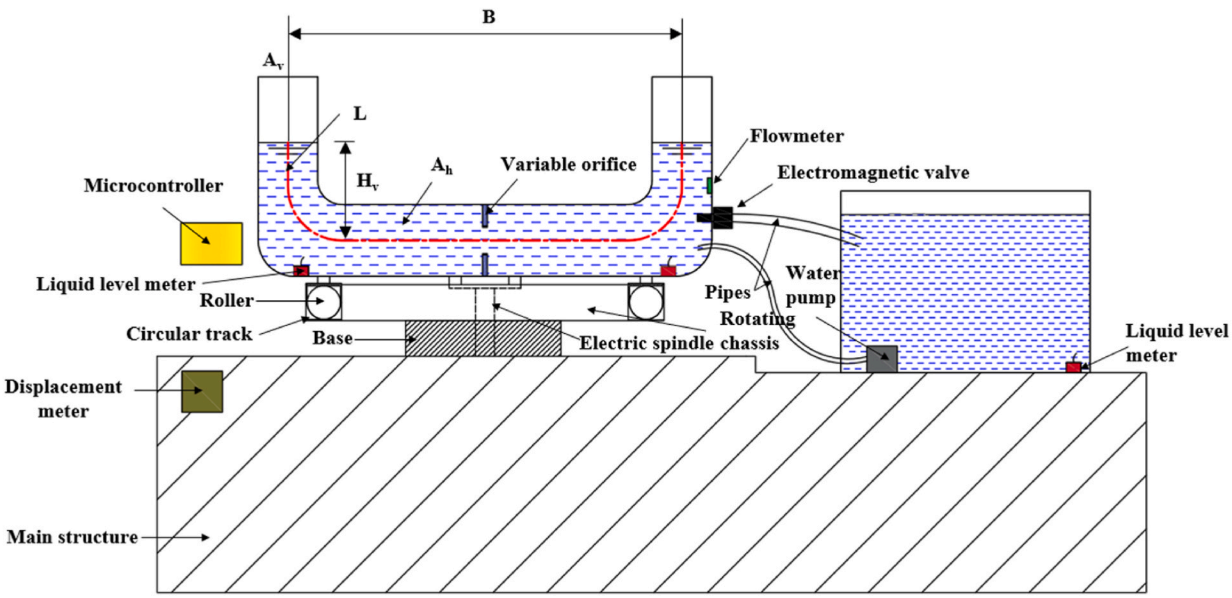

Fig. 2. The front view and sensor arrangement of RS-TLCD.

is related to the square of the liquid velocity.

2.2. Electromechanical device of RS-TLCD

Passive TLCDs have limitations in achieving optimal control effects under seismic excitations due to their inability to adjust their parameters. To improve the control effect, a semi-active control system within TLCD enabling real-time adjustments to its frequency and damping is proposed in this section. Additionally, structural designs often result in a misalignment between the mass center and stiffness center because of functional requirements, leading to translational-torsional coupling responses within the plane under external excitations. While existing studies typically utilize multiple dampers for controlling translational-torsional coupling vibration, the RS-TLCD presented in this paper comprises a single integrated liquid damper electromechanical system. Based on the variable frequency and damping capabilities of S-TLCD, the RS-TLCD incorporates a rotatable base, allowing further adjustment to align with the structural dominant vibration direction. This enhancement aims to improve control force efficiency, achieving superior intelligent control effects for translational-torsional coupling under seismic excitations, while also reducing costs and minimizing space occupation within the building.

The front view and sensor layout diagram of RS-TLCD are illustrated in Fig. 2. The U-shaped tube section of the RS-TLCD is connected to a reserve water tank placed adjacent to the TLCD. The maximum liquid level of the reserve tank should be lower than the bottom of the TLCD for liquid circulation, facilitating adjustments to the liquid column height and natural frequency of RS-TLCD. The bottom of the RS-TLCD is equipped with a rotating chassis driven by dynamic system. Liquid level meters are installed at the bottom of the vertical pipe sections on both ends of the U-shaped tube to measure the liquid level of TLCD. Flowmeters are positioned near the liquid surface of the U-shaped tube for measuring the internal liquid flow rate. Displacement meters are installed on the main structure to capture instantaneous vibration signals which are received and processed by microcontroller. Additionally, liquid level meter is installed at the bottom of the reserve tank to monitor the liquid level. If the liquid level falls below a predefined threshold, microcontroller will send a signal indicating the need for liquid replenishment.

The rotating chassis of the RS-TLCD is fixed to an electric spindle, which is embedded in the base. A circular track is affixed to the base, and the entire RS-TLCD device is secured to the main structure via this base. Rollers are installed at the bottom of the vertical sections of the U-shaped tube, allowing them to roll along the circular track. As the rollers move, they facilitate the rotation of the U-shaped tube with the rotating chassis, adjusting the angle $\theta(t)$ with respect to the X-axis in the horizontal plane. The design minimizes friction during rotation, enabling swift angle adjustments. Through variable rotational angle $\theta(t)$, RS-TLCD can rotate to the dominant vibration direction and contribute the greatest control force.

Inside the reserve water tank, a water pump is installed, connected to the U-shaped tube via a water pipe. When the liquid level inside the U-shaped tube is too low, water can be pumped into it. Additionally, there is a water pipe with an electromagnetic valve connecting the reserve tank and the U-shaped tube. If the water level in the U-shaped tube becomes too high, the electromagnetic valve can be opened, allowing the liquid to flow back into the reserve tank by gravity. Meanwhile, the pump can draw water into the reserve water tank to enhance the efficiency of liquid level regulation. By pumping liquid into the system and controlling the flow back into the reserve tank with the electromagnetic valve, the height of the liquid column in the U-shaped tube can be adjusted, thereby changing the natural frequency of RS-TLCD. To enable precise adjustments to the damping characteristic of RS-TLCD, the size of the variable orifice can be freely controlled achieving through electric valve, and the microcontroller manages its aperture. When the damping required is reduced, the microcontroller can increase the size of the variable orifice; and when the required damping is increased, the variable orifice can be reduced in the same way. The top view and sensor layout diagram of the RS-TLCD are shown in Fig. 3.

The RS-TLCD device proposed in this section is capable of simultaneously controlling the bi-directional translational-torsional

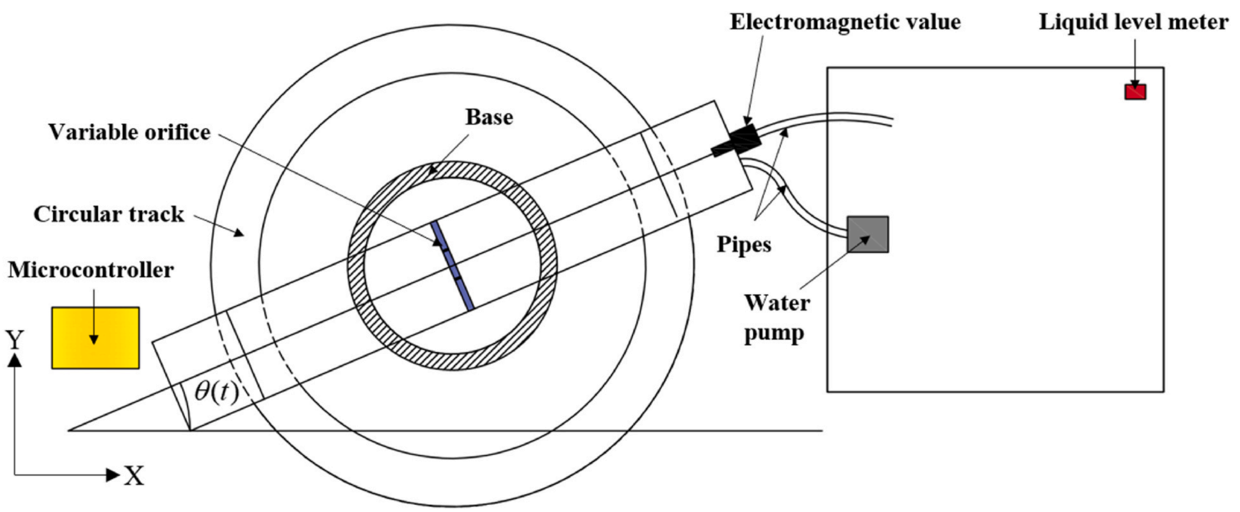

Fig. 3. The top view and sensor arrangement of RS-TLCD.

coupling responses of the structure. It exhibits several superiorities, including robust performance, high utilization efficiency of damper control force, and strong adaptive capabilities.

2.3. Control algorithm

The control performance of TLCD is dependent on its frequency and damping characteristics. Based on dynamic properties of TLCD, its frequency can be adjusted by modifying its equivalent length. Additionally, damping adjustments can be achieved by varying the size of internal orifice or altering the cross-sectional area ratio between horizontal and vertical segments. However, as a passive system, the conventional TLCD lacks the capability to adjust its parameters during operation. Consequently, its control performance may significantly deteriorate under conditions such as changes in structural frequency or the simultaneous presence of multiple external excitations, while it can only control vibrations unidirectionally. To address these limitations, the integration of semi-active devices becomes necessary to enable real-time adaptive parameter adjustments for bi-directional control.

The RS-TLCD proposed in this paper can adjust its own parameters based on the real-time identification of structural instantaneous vibrational frequency. To enable RS-TLCD to control the bi-directional translational and torsional responses in real-time, the micro-controller in this device can collect instantaneous vibration responses of main structure under external excitations through displacement meters arranged on the top floor. Wavelet transform (WT) is employed to capture and identify the bi-directional instantaneous vibration frequencies $\omega(t)$ in real-time [41–43]. Then, Equation (9) is used to convert these frequencies into the corresponding ideal hydrostatic liquid level heights, and the driving system is controlled to adjust the liquid column height of RS-TLCD. Considering the efficiency of driving system, frequency in X direction $\omega_{dx}(t)$ can be obtained according to the following equation:

$$\omega_{dx}(t) = \begin{cases} \omega_{dx\ \min} & (\omega(t) < \omega_{dx\ \min}) \\ \omega(t) & (\omega_{dx\ \min} \le \omega(t) \le \omega_{dx\ \max}) \\ \omega_{dx\ \max} & (\omega(t) > \omega_{dx\ \max}) \end{cases} \tag{10}$$

where $\omega_{dx\ \max}$ and $\omega_{dx\ \min}$ are preset maximum and minimum values of the variable frequency range in X direction. The equation of Y direction $\omega_{dy}(t)$ is similar to Equation (10).

Because RS-TLCD needs to control bi-directional translational responses in the plane and torsional responses simultaneously using only one device, it is necessary to comprehensively consider structural responses in both directions to determine the ideal tuning frequency for the final balanced bi-directional vibration state. Therefore, the final natural frequency at this moment will be calculated by weighting the absolute values of maximum displacements in both directions to achieve bi-directional balance, and the specific calculation formula is represented as follows:

$$\omega_d(t) = \frac{|D_y(t)|\omega_{dy}(t) + |D_x(t)|\omega_{dx}(t)}{|D_y(t)| + |D_x(t)|} \tag{11}$$

where $D_x(t)$ and $D_y(t)$ represent the real-time X and Y directional displacements respectively at the layer where the RS-TLCD is placed.

By using the absolute values of maximum real-time displacements in both directions of structure as weights, RS-TLCD is capable of comprehensively considering the bi-directional responses and selecting the optimal natural frequency that can simultaneously control the bi-directional vibration. Considering the time delay effect in the dynamic system, in practical application, the frequency adjustment time interval for RS-TLCD is set to Δt_f.

The variable damping function of RS-TLCD is achieved by changing the size of variable orifices. In this paper, a variable damping control strategy which can balance the instantaneous optimal parameters in both X and Y directions for bi-directional adjustment [44] is conceived, which is an extension of output signal based variable damping control algorithm proposed in Ref. [45]. Based on the instantaneous vibration responses collected by displacement meters, the microcontroller can calculate the instantaneous velocities $v_{nx}(t)$ and $v_{ny}(t)$ respectively in X and Y directions, together with the instantaneous accelerations $a_{nx}(t)$ and $a_{ny}(t)$ in both directions of the nth layer. Combined with the flow meter inside RS-TLCD, the liquid velocity $v_d(t)$ can be obtained. The calculation formula for the variable damping control algorithm of RS-TLCD is shown as follows:

$$\begin{cases} [v_{dx}(t) - v_{nx}(t)] \times a_{nx}(t) \le 0 \quad and \quad [v_{dy}(t) - v_{ny}(t)] \times a_{ny}(t) \le 0 \quad => c_d(t) = c_{\min} \\ [v_{dx}(t) - v_{nx}(t)] \times a_{nx}(t) > 0 \quad and \quad [v_{dy}(t) - v_{ny}(t)] \times a_{ny}(t) > 0 \quad => c_d(t) = c_{\max} \\ [v_{dx}(t) - v_{nx}(t)] \times a_{nx}(t) \le 0 \quad and \quad [v_{dy}(t) - v_{ny}(t)] \times a_{ny}(t) > 0 \quad => c_d(t) = c_{opt} \\ [v_{dx}(t) - v_{nx}(t)] \times a_{nx}(t) > 0 \quad and \quad [v_{dy}(t) - v_{ny}(t)] \times a_{ny}(t) \le 0 \quad => c_d(t) = c_{opt} \end{cases} \tag{12}$$

where $v_{dx}(t)$ denotes the projection velocity of liquid flow in the horizontal section of RS-TLCD in X direction, $v_{dy}(t)$ denotes its projection velocity in Y direction; $c_{\min}$ and $c_{\max}$ are the preset minimum and maximum damping coefficient respectively, c_{opt} represents the preset optimal damping coefficient.

The size of orifices within the horizontal segment of RS-TLCD can be adjusted by the microcontroller based on the relationship among the projection X and Y directional velocities and velocities and accelerations of the nth layer in the corresponding directions. Specifically, when the difference between the projection X and Y directional velocities and the X and Y directional velocities of the nth layer is in the same direction as the X and Y directional accelerations of the nth layer respectively, the orifice is reduced, causing the damping coefficient to be the preset maximum value. Conversely, when the difference is in the opposite direction of accelerations, the orifice is increased, resulting in the damping coefficient being set to the preset minimum value. In all other cases, the size of orifice is returned to its initial value, resulting in the damping coefficient being equal to the preset optimal value. It is important to note that the speed of changing damping coefficient by altering the size of orifice is greater than that of changing the frequency by varying the liquid column height. Therefore, considering the time delay effect, it is set $\Delta t_c < \Delta t_f$ in numerical simulation. It ensures that RS-TLCD can adjust its damping characteristic dynamically and effectively in response to changes of structural vibrations, providing the best bi-directional vibration control force.

The microcontroller in RS-TLCD can calculate the optimal vibration control angle based on the instantaneous vibration response collected by the displacement meter arranged on structure, using a rotating angle algorithm. In addition, the rotation of the electric shaft for bi-directional control within the plane is also controlled by the microcontroller. The calculation formula for the rotation angle algorithm proposed in this section is shown as follows:

$$\theta(t) = \arctan\left(\frac{D_{y\,\max}(t - \Delta t_R : t)}{D_{x\,\max}(t - \Delta t_R : t)}\right) \tag{13}$$

where Δt_R is the rotating angle time interval set to account for the time delay effect, $D_{x\,\max}(t - \Delta t_R : t)$ is the maximum X directional displacement within time period Δt_R before time t, and $D_{y\,\max}(t - \Delta t_R : t)$ is the maximum Y directional displacement within time period Δt_R before time t.

The rotating angle algorithm comprehensively considers the structural response bi-directionally. By using the combined direction of the maximum displacement response of structure within a certain time period as the final rotating angle for RS-TLCD, it can fully utilize RS-TLCD and minimize the bi-directional vibration response of structure to the greatest extent.

In summary, the proposed control algorithm of RS-TLCD with variable frequency, damping and angle is summarized in Fig. 4.

In Fig. 4, RS-TLCD is capable of identifying the instantaneous vibration frequency of structure based on WT through the displacement meter signal in X and Y direction. The final frequency of RS-TLCD is calculated using Equation (11) with weighting factors to adjust its frequency at that moment. Then comparing actual liquid level measured by liquid level meters and ideal liquid level obtained from Equation (9), the microcontroller is able to make decisions to control the pump and the electromagnetic valve for liquid level adjustment. Additionally, a comprehensive analysis is conducted based on Equation (12) to judge the relationship among the acceleration and velocity responses of main structure and the projection velocity responses of RS-TLCD in two directions. This analysis is presented to adjust the damping coefficient of RS-TLCD. The optimal rotating angle is determined through Equation (13) based on the combined direction of the maximum displacement response of structure within a certain time period. Then the microcontroller drives the electric spindle to achieve changes in angle of rotating chassis. Therefore, RS-TLCD can achieve intelligent bi-directional translational and torsional vibration control within the structural plane. It also can be known from Fig. 4 that the combined

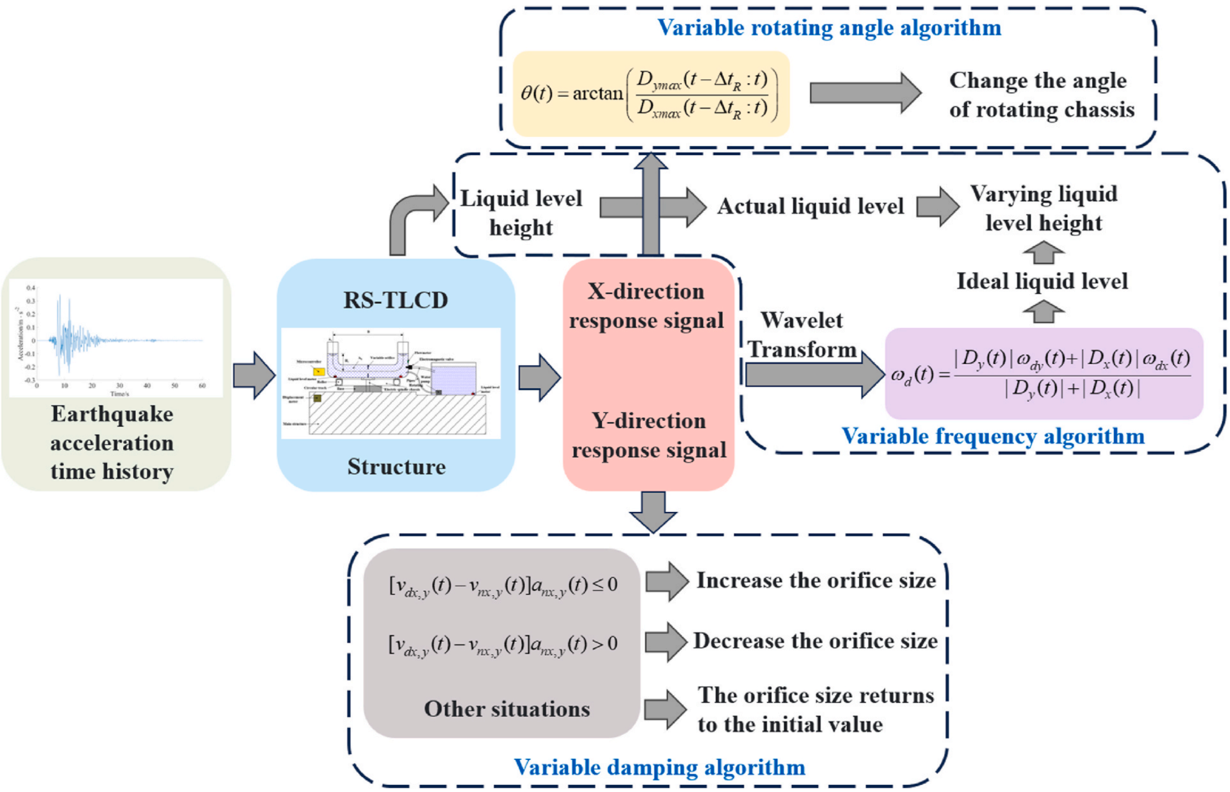

Fig. 4. Combined variable frequency, damping and angle control algorithm of RS-TLCD.

control algorithm is only based on output measured signals from the health monitoring system, no structural modal information and earthquake records are needed.

3. Equations of motion and numerical model introduction

3.1. Equations of motion

To verify the earthquake mitigation performance of proposed RS-TLCD and highlight its control effect, for comparison, cases without control, with two optimal X and Y directional passive TLCDs arranged respectively and two unidirectional S-TLCDs with variable liquid column height and damping are given. Among these cases, dynamic calculation diagrams of three structural systems with controllers are presented in Fig. 5 respectively.

For instance, the dynamic equation of RS-TLCD case in Fig. 5(c) is able to be expressed as:

$$\mathbf{M}\ddot{\mathbf{U}} + \mathbf{C}\dot{\mathbf{U}} + KU = -ME\ddot{\mathbf{U}}_{\mathbf{g}} \tag{14}$$

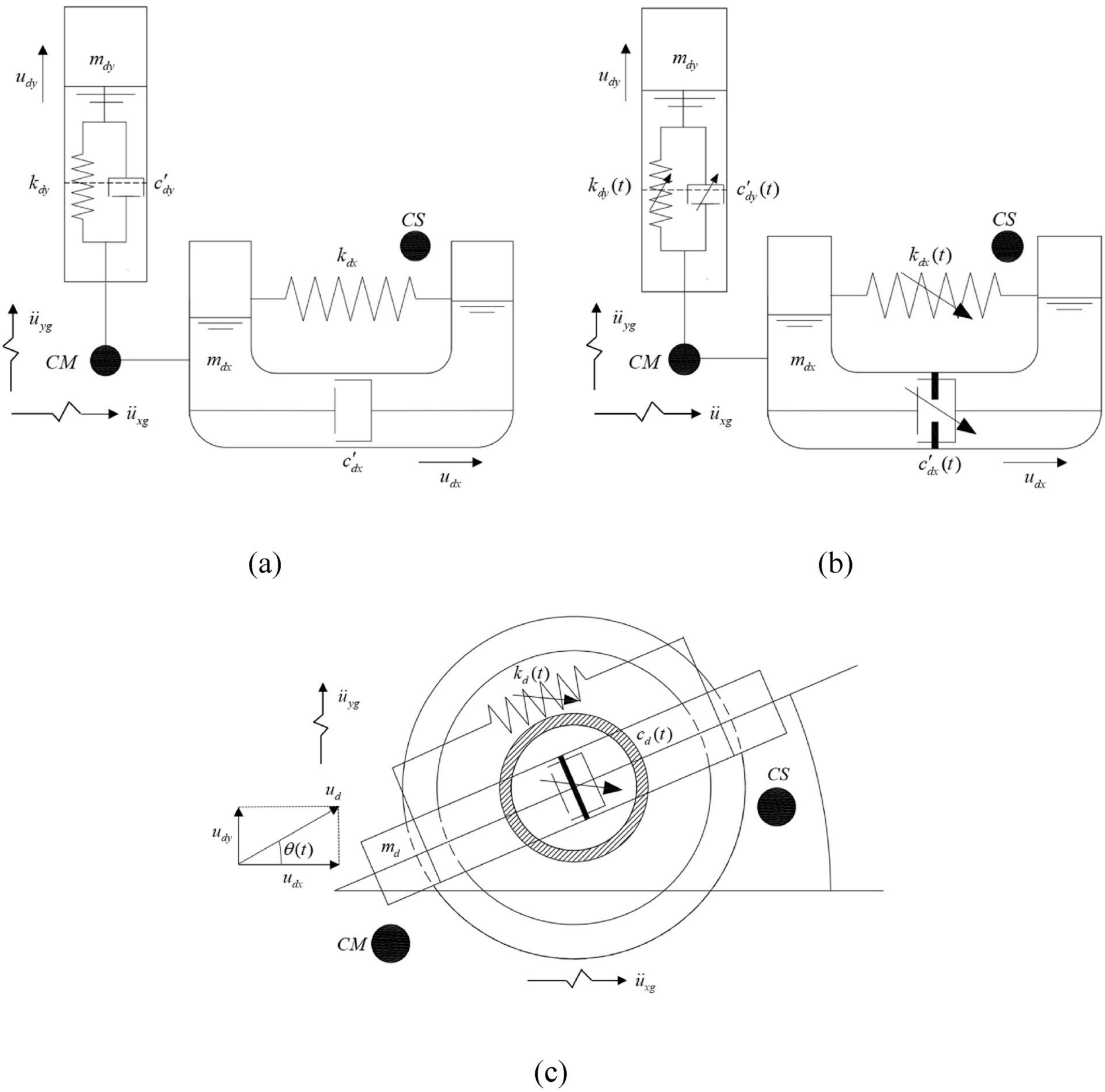

Fig. 5. Comparison cases. (a) Two optimal passive TLCDs; (b) Two unidirectional S-TLCDs; (c) RS-TLCD.

where $\mathbf{M}$, $\mathbf{C}$ and $\mathbf{K}$ denote mass, damping and stiffness matrixes of system respectively; $\mathbf{U}$, $\dot{\mathbf{U}}$ and $\ddot{\mathbf{U}}$ are displacement, velocity and acceleration state vectors respectively; $\mathbf{E}$ and $\ddot{\mathbf{U}}_\mathbf{g}$ represent the conversion matrix and bi-directional seismic acceleration respectively. The preceding related matrixes in Equation (14) are shown as follows.

$$\mathbf{M} = diag\left[\mathbf{M}_x, \mathbf{M}_y, \mathbf{M}_\theta\right] \tag{15}$$

$$\mathbf{M}_x = diag[m_1, m_2, \cdots m_n, m_{dx}] \tag{16}$$

$$\mathbf{M}_y = diag\left[m_1, m_2, \cdots m_n, m_{dy}\right] \tag{17}$$

$$\mathbf{M}_\theta = diag[J_1, J_2, \cdots J_n] \tag{18}$$

$$\mathbf{K} = \begin{bmatrix} \mathbf{K}_x & \mathbf{0} & \mathbf{K}_{x\theta} \\ \mathbf{0} & \mathbf{K}_y & \mathbf{K}_{y\theta} \\ \mathbf{K}_{\theta x} & \mathbf{K}_{\theta y} & \mathbf{K}_\theta \end{bmatrix} \tag{19}$$

$$\mathbf{K}_x = \begin{bmatrix} k_{x1}+k_{x2} & -k_{x2} & & & & \\ -k_{x2} & k_{x2}+k_{x3} & -k_{x3} & & & \\ & -k_{x3} & \ddots & \ddots & & \\ & & \ddots & k_{x(n-1)}+k_{xn} & -k_{xn} & \\ & & & -k_{xn} & k_{xn}+\dfrac{2m_{dx}g}{H_{vL}+H_{vR}+\lambda B}\cos\theta(t) & -\dfrac{2m_{dx}g}{H_{vL}+H_{vR}+\lambda B}\cos\theta(t) \\ & & & & -\dfrac{2m_{dx}g}{H_{vL}+H_{vR}+\lambda B}\cos\theta(t) & \dfrac{2m_{dx}g}{H_{vL}+H_{vR}+\lambda B}\cos\theta(t) \end{bmatrix} \tag{20}$$

$$\mathbf{K}_{x\theta} = \mathbf{K}_{\theta x}^{\mathrm{T}} = \mathbf{K}_x e_y \tag{21}$$

$$\mathbf{K}_{y\theta} = \mathbf{K}_{\theta y}^{\mathrm{T}} = \mathbf{K}_y e_x \tag{22}$$

$$\mathbf{U} = \left[u_{x1}, u_{x2}, \cdots u_{xn}, u_{dx}, u_{y1}, u_{y2}, \cdots u_{yn}, u_{dy}, u_{\theta 1}, u_{\theta 2}, \cdots u_{\theta n}\right]^{\mathrm{T}} \tag{23}$$

$$c_{dx}(t) = \frac{1}{2}\rho \frac{{A_v}^2}{A_h}\delta|\dot{u}_{dx}| \tag{24}$$

$$\ddot{\mathbf{U}}_g = \left[\ddot{u}_{xg}, \ddot{u}_{yg}\right]^{\mathrm{T}} \tag{25}$$

where $\mathbf{M}_x$, $\mathbf{M}_y$ and $\mathbf{M}_\theta$ are X directional, Y directional and torsional mass matrixes of the system implemented with RS-TLCD respectively; m_i and J_i mean the mass and rotational inertia of the ith story respectively; $m_{dx} = m_d \cos\theta(t)$ and $m_{dy} = m_d \sin\theta(t)$ are the equivalent mass of RS-TLCD in two directions respectively, m_d represents the participating mass of RS-TLCD; In Equation (19), $\mathbf{K}_x$, $\mathbf{K}_y$ and $\mathbf{K}_\theta$ denote X directional, Y directional and torsional stiffness matrixes respectively; $\mathbf{K}_y$ and $\mathbf{K}_\theta$ can be obtained similarly by referring to Equation (20); k_{xi} and $k_{dx}(t) = \frac{2m_{dx}g}{H_{vL}+H_{vR}+\lambda B}\cos\theta(t)$ represent the translational stiffness in X direction of the ith story and the equivalent real-time stiffness of RS-TLCD in X direction respectively, while H_{vL} and H_{vR} are hydrostatic liquid level heights in the left and right vertical segment of RS-TLCD respectively; $\mathbf{K}_{x\theta}$ and $\mathbf{K}_{y\theta}$ are translational-torsional coupling matrixes in two directions respectively; e_x and e_y represent eccentricities of main structure in two directions respectively; damping matrix $\mathbf{C}$ is constructed by Rayleigh damping model in a similar manner, with the addition of X and Y directional real-time damping coefficients of RS-TLCD $c_{dx}(t)$ and $c_{dy}(t)$ which can be obtained by Equation (24); u_{xi}, u_{yi} and $u_{\theta i}$ represent X directional, Y directional and torsional displacements of the ith story respectively; u_{dx} and u_{dy} are X and Y directional displacements of RS-TLCD respectively; $\ddot{u}_{xg}$ and $\ddot{u}_{yg}$ represent seismic accelerations in two directions respectively.

Based on the above equations of motion, numerical simulation and comparative studies can be conducted for the translational-torsional coupling vibration control in eccentric buildings with different types of TLCDs implemented. By parameters including the mass, stiffness, damping, and eccentricity of the selected main structure, a theoretical calculation model can be established. Utilizing the semi-active control algorithm proposed in Section 2.3, the performance of RS-TLCD device, introduced in Section 2.2, the coupled bi-directional vibration control effect under seismic excitations can be verified.

3.2. Numerical model introduction

A thirty-story bi-directional eccentric frame structure is proposed as a case study, whose width is 16 m and length is 48 m [46]. This paper conducts a comparative study on the vibration control performance under bi-directional seismic excitation, utilizing MATLAB to verify the intelligent vibration mitigation control performance of RS-TLCD proposed in Section 2, particularly in terms of its coupled translational-torsional behavior under bi-directional seismic excitations.

Masses of each floor in the bi-directional eccentric frame structure are all set to 9.216×10^5 kg, with a rotational inertia of 2.797×10^8 kg • m^2 for each floor. X and Y directional stiffness coefficients of the bottom floor are both set to 1.021×10^9 N • m^{-1}, while stiffness coefficients for remaining floors in two directions are all set to 1.6213×10^9 N • m^{-1}. The torsional stiffness coefficient of bottom floor is 3.1651×10^{11} N • m • rad^{-1}, and torsional stiffness coefficients for the other floors are all set to 5.0261×10^{11} N • m • rad^{-1}. The structural geometric center and stiffness center are coincident. The X directional eccentricity e_x is 6 m, and the eccentricity in Y direction e_y is 2 m. The structural modal damping ratio is taken as 2 %. Using the mode decomposition method, it is found that the natural frequencies in two directions of the thirty-story bi-directional eccentric frame structure are equal. The first ten natural frequencies are listed in Table 1. Besides, first modal mass participation coefficients in two directions are both 83.76 %.

15 representative bi-directional seismic waves with different spectral characteristics from Ref. [47] are selected for the simulation. To avoid the impact of different amplitude values of seismic acceleration on the discussion of calculation results, the amplitude of seismic acceleration is normalized and uniformly adjusted to minor earthquake acceleration amplitude 35 cm/s^2 according to Chinese code. The selected bi-directional seismic waves are shown in Table 2.

The numerical simulation will consider four cases in total, which are without control, with two X and Y directional passive TLCDs respectively, with two unidirectional S-TLCDs, and with one RS-TLCD implemented.

For the passive TLCD in Fig. 5 (a), the mass in each direction is set to 2 % of the first modal mass of selected model, which is 463178 kg. The natural frequency is set equal to the first natural frequency of selected model, which is 0.3373 Hz.

For the S-TLCD in Fig. 5 (b), the mass in each direction is consistent with the passive TLCD. And the variable frequency range is ±5 % of the first natural frequency of selected model, which is [0.3204 Hz, 0.3542 Hz], then the corresponding effective length range is [3.957m, 4.834m]. Considering the time delay effect of dynamic system, the time interval for frequency variation Δt_f is set to 2.6 s, which is slightly shorter than the first natural period of selected structure. To ensure that the TLCD horizontal section is always filled with liquid during frequency adjustment, the cross-sectional area ratio λ between the vertical and horizontal sections of TLCD is set to 0.231.

Because the nonlinear damping of TLCD is related to the flow rate of the liquid, it is difficult to accurately provide the adjustment range of variable damping. In this case, the damping adjustment is achieved by varying ratio κ in Equation (6) using variable orifice in the horizontal section of TLCD. The initial value of κ is set to 0.4, with an adjustable range of [0.1, 0.8]. Similarly, considering the time delay effect, the time interval for variable damping is set to 1 s.

For RS-TLCD with bi-directional arrangement shown in Fig. 5 (c), the variable frequency range, variable damping range, time interval are all consistent with unidirectional S-TLCD. The participation mass ratio of RS-TLCD to unidirectional S-TLCD is 1.5, which means that the participation mass of RS-TLCD is set to 694767 kg. The cross-sectional area ratio λ between the vertical and horizontal sections of RS-TLCD is set to 0.237. The angle variation interval of rotating chassis is set to be consistent with the frequency variation interval, so that the damper can change both angle and frequency simultaneously to achieve better vibration control performance. The initial placement angle $\theta(t)$ of RS-TLCD is 0°, which is aligned with X direction in the plane.

In summary, parameters for cases with dampers are summarized in Table 3.

There are three kinds of semi-active control systems in this paper, which are variable frequency, variable damping, and variable angle systems respectively. In the following, the time delay of three systems will be explained in detail.

For time delay during frequency variation, the water pump needs time to pump water to reach the desired liquid column height for frequency matching. For the case study in section 3.2, the variable frequency range is [0.3204 Hz, 0.3542 Hz], then the corresponding effective length range is [3.957 m, 4.834 m], which means that the maximum water volume needed to be pumped is 27.082 m^3. The semi-active TLCD in this paper focuses on the first-order period of the structure which is 3.0 s, therefore, the response time of the actuator can be slightly less than the first-order period which is set to 2.6 s. Then the pump water speed of 10.42 m^3/s is required. Two water pumps with a motor power of 500 kW and a pumping capacity of 18,800 cubic meters per hour can pump water at the speed of 10.44 m^3/s which is faster than the required speed. Therefore, the time delay for frequency adjustment is set to 2.6 s. Using a higher-power pump or multiple pumps can achieve faster speed.

For time delay during damping variation, the adjustment of orifices can be achieved through the opening and closing of electric valve, which acts within a second. Hence, the time for the valve to reach the predetermined position is set to 1 s in this paper, which means the time interval for damping variation.

For time delay during angle variation, it is caused by the rotational speed limit of the rotating chassis. The existing rotating chassis can rotate at a speed of 30° per second with a motor power of 600 kW. Using a higher-power motor or multiple motors can achieve faster speed.

By analyzing the dynamic response of main structure under bi-directional seismic actions, based on dynamic equations in Section 3.1 and specific parameters in Table 3, numerical simulation is proposed to prove the bi-directional translational-torsional coupling

Table 1
Structural natural frequencies in X and Y directions/Hz.

First	Second	Third	Fourth	Fifth	Sixth	Seventh	Eighth	Ninth	Tenth
0.3373	1.0112	1.6831	2.3517	3.0155	3.6729	4.3221	4.9615	5.5892	6.2034

Table 2
Selected bi-directional seismic waves.

Serial number	Station	The name of seismic wave	
		X-direction	Y-direction
1	El Centro Array #11	IMPVALL-E11140	IMPVALL-E11230
2	Aeropuerto Mexicali	IMPVALL-AEP045	IMPVALL-AEP315
3	El Centro Differential Array	IMPVALL-EDA270	IMPVALL-EDA360
4	Brawley Airport	IMPVALL-BRA225	IMPVALL-BRA315
5	EC County Center FF	IMPVALL-ECC002	IMPVALL-ECC092
6	El Centro Array # 10	IMPVALL-E10050	IMPVALL-E10320
7	Agrarias	IMPVALL-AGR003	IMPVALL-AGR273
8	El Centro Array #5	IMPVALL-E05140	IMPVALL-E05230
9	El Centro Array #7	IMPVALL-E07140	IMPVALL-E07230
10	El Centro Array #8	IMPVALL-E08140	IMPVALL-E08230
11	El Centro Array #3	IMPVALL-E03140	IMPVALL-E03230
12	Holtville Post Office	IMPVALL-HVP225	IMPVALL-HVP315
13	Pacoima Dam	NORTHR-PAC175	NORTHR-PAC265
14	KJMA	KOBE-KJM000	KOBE-KJM090
15	CHY006	CHICHI-CHY006-N	CHICHI-CHY006-W

Table 3
Parameter summary for cases with dampers.

Case	Total mass	λ	κ	Interval of frequency variation	Interval of damping variation	Interval of angle variation
Passive TLCD	2.0×463178 kg	0.231	0.4	None	None	None
S-TLCD	2.0×463178 kg	0.231	[0.1, 0.8]	2.6 s	1 s	None
RS-TLCD	1.5×463178 kg	0.237	[0.1, 0.8]	2.6 s	1 s	2.6 s

control performance of RS-TLCD.

4. Numerical simulation

Under seismic excitations, the safety evaluation of main structure adopts a comparative analysis using the maximum value X_{emax} and root mean square (RMS) value X_{erms} of the structural X and Y directional top-layer displacement and the structural torsion angle. Therefore, totally six indexes are compared.

In addition, seismic mitigation rate is used to highlight the improved vibration control performance of RS-TLCD compared to the other two control cases.

4.1. Results comparison

Six indicators are employed in the dynamic response analysis of main structure under bi-directional seismic excitations to comparatively analyze the seismic mitigation performance of different control cases, including the maximum and RMS values of displacement in two directions at the top story, as well as the maximum and RMS values of torsion angle, which can be denoted as

Table 4
Comparison of structural X directional displacement response of the top story.

No.	$X_{x,\text{emax}}$/cm				$X_{x,\text{erms}}$/cm			
	Without control	Passive TLCD	S-TLCD	RS-TLCD	Without control	Passive TLCD	S-TLCD	RS-TLCD
1	4.484	3.410	3.670	3.305	2.044	1.247	1.308	1.184
2	4.406	3.733	3.738	3.615	2.080	1.559	1.567	1.400
3	7.028	6.373	6.202	6.138	3.023	1.674	1.513	1.474
4	10.040	8.981	8.909	8.663	4.109	2.437	2.821	2.184
5	5.801	5.640	5.651	5.630	1.655	1.583	1.535	1.388
6	12.104	10.588	11.691	10.261	5.551	3.206	3.775	2.888
7	4.338	3.508	3.795	3.588	1.773	1.312	1.272	1.264
8	10.373	6.528	5.533	6.737	3.861	2.096	1.796	2.115
9	8.059	6.113	6.439	6.228	3.414	2.023	1.965	1.974
10	3.242	2.703	2.723	2.771	1.449	0.887	0.952	0.935
11	7.676	6.786	7.159	6.906	2.683	1.888	1.916	1.858
12	6.996	6.584	6.724	6.676	2.916	2.061	2.088	1.899
13	1.610	1.291	1.326	1.290	0.856	0.481	0.492	0.476
14	2.098	1.997	1.969	1.980	0.569	0.310	0.315	0.263
15	5.086	4.204	4.717	4.393	1.336	1.236	1.096	1.084

$X_{x,emax}$, $X_{y,emax}$, $X_{x,erms}$, $X_{y,erms}$, $X_{\theta,emax}$, $X_{\theta,erms}$ respectively. Calculation results are shown in Tables 4–6 and Fig. 6 respectively. To highlight the improved effectiveness of RS-TLCD compared to the other two types of TLCDs, response reductions compared to the case without control are presented in Fig. 7.

From Tables 4–6 and Fig. 6, it can be observed that although structural dynamic characteristics in two directions are the same, structural displacement responses in two directions are quite different due to the different eccentricity and the different seismic characteristics in two directions. In addition, because the structural eccentricity in X direction is three times that in Y direction, its Y directional dynamic response is more susceptible to torsion. Compared with the X directional displacement response, the Y directional displacement response distribution characteristics under different seismic waves are more similar to the torsion response.

It can be seen in Fig. 7 that generally, the three TLCDs all have good earthquake mitigation effect, and the control performance of RMS response is superior than the maximum. Because Y direction is more susceptible to torsion than X direction, X directional displacement control performance is better than that in Y direction. For both X and Y directional responses with two unidirectional S-TLCDs, reduction rates of various indicators are better than those with passive TLCDs. Meanwhile, reduction rates of indicators with an RS-TLCD are generally similar to those with two unidirectional S-TLCDs. In addition, it is worth mentioning that in terms of controlling the maximum and RMS values of torsional angle, the energy dissipation and seismic mitigation ability of RS-TLCD is superior to that of S-TLCDs case in both X and Y directions. This strongly indicates that RS-TLCD can effectively mitigate the coupled translational and torsional dynamic response of bi-directional asymmetric structure under bi-directional seismic excitations, especially in terms of torsional response control.

It is worth noting that the RS-TLCD proposed only requires a single device for bi-directional and torsional vibration control of the structure compared with the S-TLCD and passive TLCD, while the S-TLCD and passive TLCD require multiple devices and more participating mass. The participating mass ratio of S-TLCDs and passive TLCDs are both 2, while the participating mass ratio of RS-TLCD is only 1.5.

According to Fig. 7, the control effect of RS-TLCD on the RMS value of displacement response is significantly better than the maximum value, and better than passive TLCDs in general. It is close to the control performance of two unidirectional S-TLCDs, and even performs better under specific earthquakes. In terms of torsion resistance, RS-TLCD has the best control performance on the whole, such as the effects of No. 2, 5, 8 and 14 seismic waves. Due to the nonlinearity of damping, RS-TLCD has better control performance under the action of seismic waves that cause larger structural response. In addition, according to the average seismic reduction of six indicators including maximum and RMS values of X and Y directional displacements and rotation angle under the action of 15 earthquake waves in Table 7, it can be seen that though RS-TLCD only uses a single device with smaller participating mass, its control effect is better than that of S-TLCD and passive TLCD.

It can be seen in Table 7 that compared to two unidirectional passive TLCDs and S-TLCDs, the improvement of proposed RS-TLCD is more significant in RMS response reduction than maximum; as for the maximum response reduction, it is more effective in Y-directional displacement control and torsional response control. Therefore, it can be known that the RS-TLCD can enhance the seismic translational-torsional coupling response control performance to a great degree.

In summary, it is indicated that RS-TLCD provides a comprehensive seismic mitigation solution, particularly in controlling torsional responses, while S-TLCDs and passive TLCDs offer more limited but still significant reductions in various indicators in Fig. 7.

4.2. Time history comparisons

To further analyze the characteristics of structural response in both time and frequency domains under seismic excitation, the 5th group with the largest torsional response among 15 groups of seismic excitations is selected as an example. Under the 5th group's seismic excitation, time history and frequency spectra comparisons of the structural top story are presented in Fig. 8.

From Fig. 8, it can be observed that for the first 8 s, the structural displacement response of structure with additional passive TLCDs,

Table 5
Comparison of structural Y directional displacement response of the top story.

No.	$X_{y,emax}$/cm				$X_{y,erms}$/cm			
	Without control	Passive TLCD	S-TLCD	RS-TLCD	Without control	Passive TLCD	S-TLCD	RS-TLCD
1	3.148	2.313	2.311	2.231	1.234	0.958	1.013	0.941
2	1.837	1.056	1.136	1.138	0.619	0.459	0.479	0.474
3	2.825	2.018	2.007	2.033	1.147	0.681	0.654	0.629
4	5.399	4.909	5.098	4.711	2.276	1.758	1.856	1.783
5	10.462	9.842	10.469	8.670	4.151	3.853	3.630	3.237
6	5.818	5.011	4.975	5.189	2.331	1.771	1.761	1.823
7	5.583	5.538	5.436	5.402	1.593	1.512	1.504	1.442
8	9.974	9.038	9.051	8.698	3.660	3.300	2.778	2.970
9	7.174	6.686	7.279	6.650	3.141	2.810	2.614	2.736
10	4.115	4.443	4.360	4.362	1.543	1.459	1.403	1.412
11	5.691	5.421	5.420	5.334	2.190	2.080	2.097	2.069
12	10.083	8.899	8.339	8.830	4.155	3.788	3.583	3.732
13	2.014	1.640	1.741	1.567	0.734	0.650	0.653	0.651
14	2.262	2.157	2.193	1.978	0.358	0.315	0.306	0.279
15	4.282	4.431	4.319	4.306	1.505	1.450	1.296	1.343

Table 6
Comparison of structural torsional angle response of the top story.

No.	$X_{\theta,\mathrm{emax}}/10^{-4}$ rad				$X_{\theta,\mathrm{erms}}/10^{-4}$ rad			
	Without control	Passive TLCD	S-TLCD	RS-TLCD	Without control	Passive TLCD	S-TLCD	RS-TLCD
1	15.492	13.582	13.649	13.405	6.053	5.127	5.349	5.050
2	7.611	6.628	6.516	5.629	2.871	2.517	2.449	2.168
3	8.432	8.423	8.324	8.383	3.029	2.612	2.870	2.638
4	28.896	26.454	26.529	26.500	10.716	10.133	9.630	10.072
5	63.364	56.350	58.892	56.164	25.416	21.657	21.421	18.237
6	26.008	22.320	22.176	23.503	8.568	8.111	7.763	8.382
7	17.292	17.224	16.303	16.812	7.146	6.893	6.641	6.546
8	63.809	56.241	56.341	53.071	21.827	18.692	16.105	16.847
9	49.680	44.712	44.722	43.398	18.759	16.060	14.758	15.151
10	23.793	22.136	22.049	21.238	8.119	7.350	6.968	6.901
11	32.990	28.536	26.370	27.237	11.728	10.598	10.711	10.438
12	62.737	54.715	57.899	54.950	24.859	21.714	21.710	20.843
13	10.493	9.122	9.284	9.203	4.299	3.664	3.747	3.576
14	10.074	9.315	9.602	9.220	1.935	1.652	1.706	1.517
15	31.919	27.918	29.846	28.872	9.544	8.485	8.177	8.021

S-TLCDs, and RS-TLCD are similar. On a broader scale, RS-TLCD exhibits the best control performance in the aspect of X and Y directional displacements. Furthermore, as shown in Fig. 8 (e), RS-TLCD demonstrates superior control effectiveness over passive TLCDs and S-TLCDs in terms of torsion angle control across all time history. Comparing and analyzing Fig. 8(b)–(d), and (f), results of spectral analysis confirm that RS-TLCD outperforms passive TLCDs and S-TLCDs in controlling displacements in X and Y directions and torsional angle.

Further, the comparison of structural displacement responses of all stories under the 5th group of bi-directional seismic excitation is shown in Fig. 9.

According to comparison results of all stories in Fig. 9, it can be inferred that in the aspect of maximum X directional displacement, the control performance of RS-TLCD and S-TLCDs are similar to that of passive TLCDs. In the field of maximum Y directional displacement, RS-TLCD demonstrates the best control effect, while passive TLCDs perform better than S-TLCDs. Regarding the maximum torsion angle, both RS-TLCD and passive TLCDs exhibit comparable control performance, which are superior to that of S-TLCDs. In terms of the RMS value of X directional displacement, RS-TLCD shows the most effective control, followed by S-TLCDs, which performs better than passive TLCDs. For the RMS value of Y directional displacement, RS-TLCD provides the best control effect, outperforming passive TLCDs and S-TLCDs. Finally, in terms of the RMS value of torsion angle, RS-TLCD again demonstrates the best reduction performance of seismic response, while the performance of S-TLCDs is similar to that of passive TLCDs. By comparing the X and Y directional displacement of all stories, it can be found that both the maximum and RMS values of displacement in Y direction are greater than those in X direction. This is due to the larger eccentricity of the main structure in X direction ($e_x = 6$ m) compared to Y direction ($e_y = 2$m), making the structural displacement in Y direction more susceptible to torsional response.

In real application, sensor failure is an inevitable situation. First of all, the RS-TLCD proposed in this paper has three functions, which are variable frequency, variable damping and variable angle respectively. The variable frequency part needs to be realized by displacement meters arranged in X and Y directions of the structure, the variable damping part uses the flowmeter in the U-shaped tube as the basis for judgment, and the variable angle part needs displacement meters in two directions of the structure as well. In real application, more displacement meters and flowmeters can be arranged to improve redundancy and prevent sensor failure from causing the system unable to achieve the semi-active control performance. On the other hand, if all sensors fail, the device will become a passive TLCD. This paper also carries out numerical simulation on passive TLCD, and results show that optimized passive TLCD also has a good control performance.

Signal noise is also an inevitable situation in practical use. Therefore, a comparative simulation using gaussian white noise with a signal to noise ratio (SNR) of 25 dB is conducted as a complement [48]. The results of seismic reduction are shown in Table 8.

Table 8 shows that the signal noise has little effect on the control performance of RS-TLCD in the displacement and torsion, and RS-TLCD still exhibits better vibration control performance compared to passive TLCD. In comparison, the control performance of S-TLCD is more affected by signal noise, and the six indicators of RS-TLCD are all superior to S-TLCD with signal noise. Hence, it can be concluded that RS-TLCD can still maintain excellent vibration control performance with signal noise contamination.

4.3. Variable parameters of semi-active controller

To further explain the principle of improved seismic performance through semi-active control, the instantaneous frequency and instantaneous orifice ratio in variable damping system with two S-TLCDs arranged in X and Y directions respectively under the 5th seismic excitation are proposed in Fig. 10. The instantaneous frequency, instantaneous orifice ratio and instantaneous angle of RS-TLCD under the same seismic excitation is illustrated in Fig. 11.

Through comparative analysis of Figs. 10(a) and 11(a), it can be observed that the natural frequencies of S-TLCDs in both directions have only two values besides the initial value, which are the maximum and minimum values within the preset frequency adjustment range comparatively. The natural frequency of RS-TLCD is determined through a balanced assessment of structural responses in both X

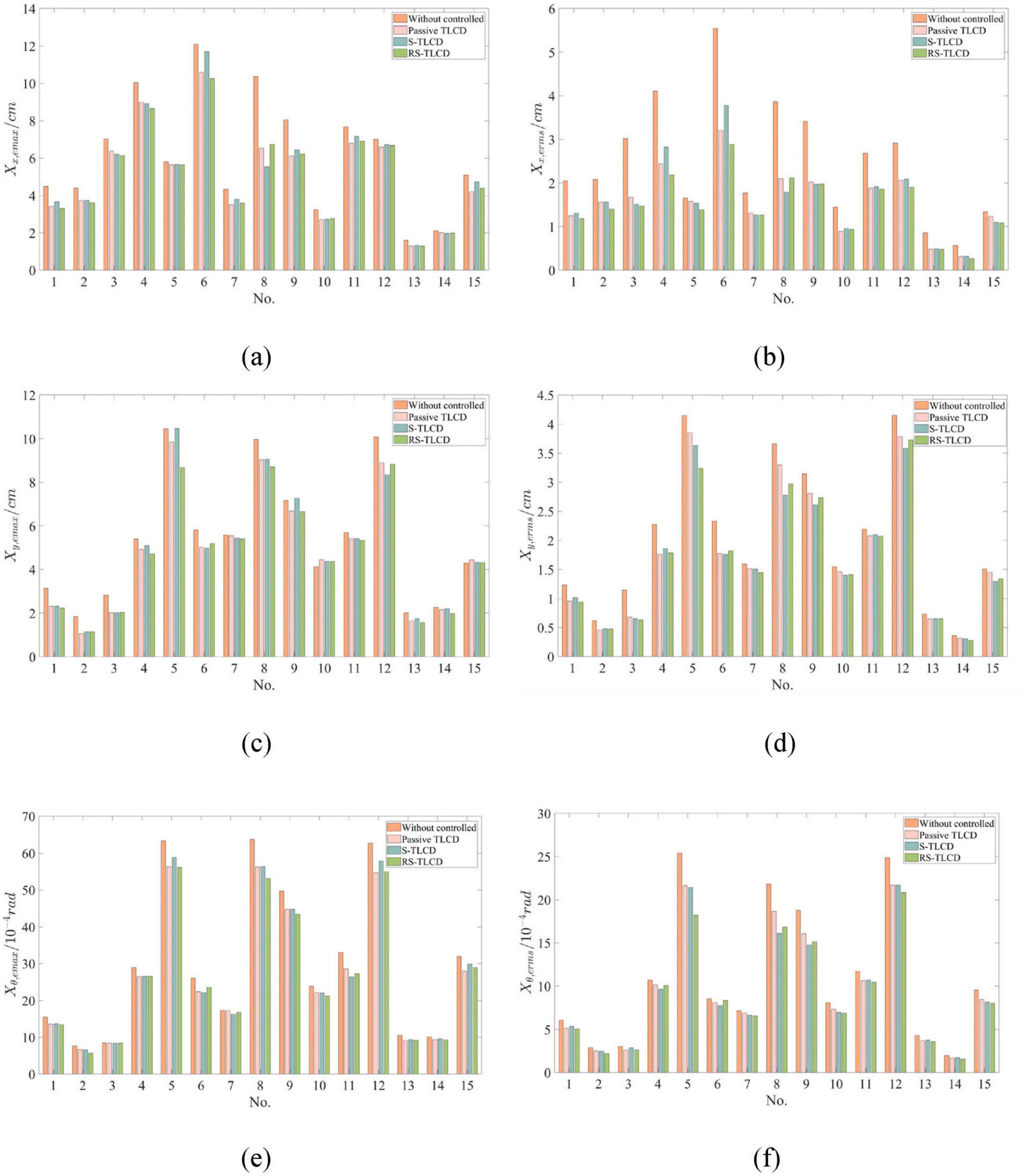

Fig. 6. The structural displacement response of the top story under seismic excitations. (a) X directional maximum; (b) X directional RMS; (c) Y directional maximum; (d) Y directional RMS; (e) Maximum torsion angle; (f) RMS torsion angle.

and Y directions. This allows for fine adjustments within the preset frequency adjustment range, enabling the natural frequency of RS-TLCD to closely align with the structural instantaneous frequency. Additionally, both S-TLCDs and RS-TLCD can adjust their variable orifices to increase or decrease orifice ratio κ based on Figs. 10(b) and 11(b) respectively, achieving damping adjustments in real time. According to Fig. 11(c), the instantaneous angle of RS-TLCD is mostly located within a specific range of $70^{\circ}\sim110^{\circ}$, indicating that RS-TLCD is often oriented towards Y direction, which is more susceptible to torsional response. This suggests that the variable rotating angle algorithm proposed in this study is capable of identifying the dominant vibration direction with larger displacement response

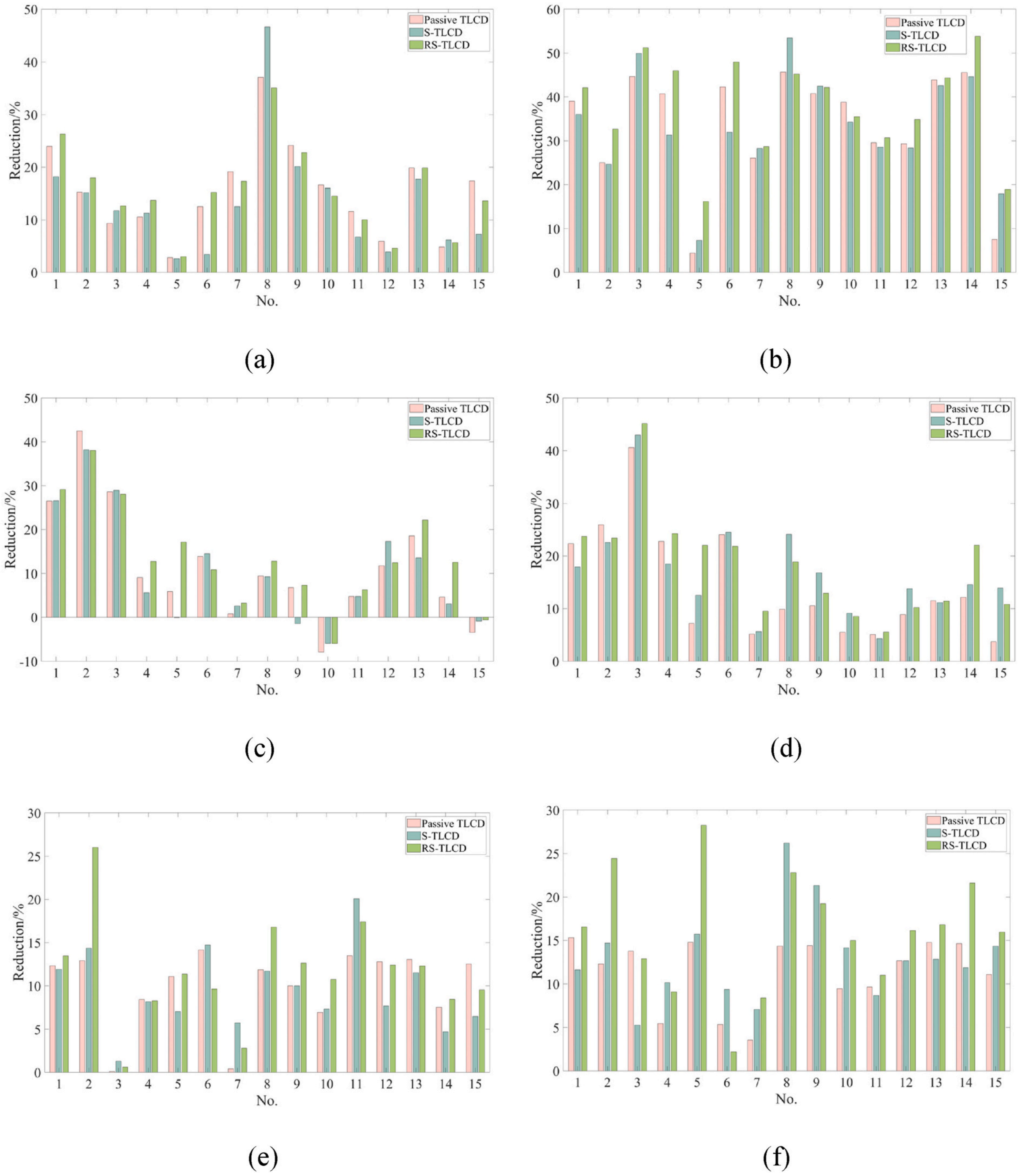

Fig. 7. The seismic reduction of different TLCDs compared to the case without control. (a) X directional maximum displacement; (b) X directional RMS displacement; (c) Y directional maximum displacement; (d) Y directional RMS displacement; (e) Maximum torsion angle; (f) RMS torsion angle.

Table 7
Average seismic reduction of three controllers under seismic excitations.

Case	$X_{x,\mathrm{emax}}$	$X_{y,\mathrm{emax}}$	$X_{\theta,\mathrm{emax}}$	$X_{x,\mathrm{erms}}$	$X_{y,\mathrm{erms}}$	$X_{\theta,\mathrm{erms}}$
Passive TLCD	15.39 %	11.45 %	9.85 %	33.54 %	14.33 %	11.43 %
S-TLCD	13.29 %	10.40 %	9.52 %	33.46 %	16.81 %	13.06 %
RS-TLCD	15.48 %	13.74 %	11.50 %	38.03 %	18.00 %	16.03 %

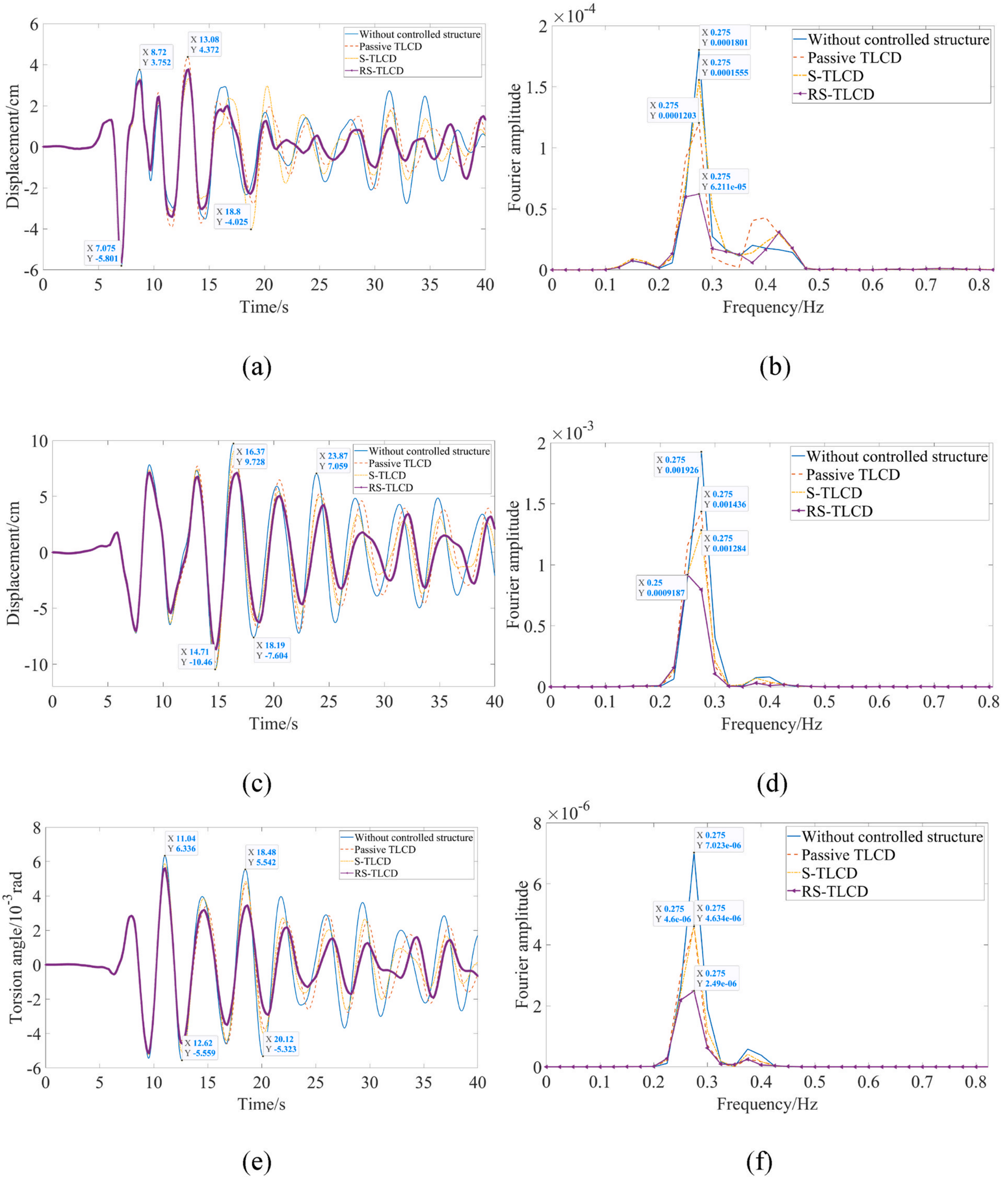

Fig. 8. Comparison of structural top story response under the 5th group of bi-directional seismic excitation. (a) Time history of X directional displacement; (b) X directional displacement spectra; (c) Time history of Y directional displacement; (d) Y directional displacement spectra; (e) Time history of Torsional angle; (f) Torsional angle spectra.

and controlling the rotation angle of RS-TLCD to achieve maximum control ability in real time, thereby improving the efficiency of output force control in the dominant direction of vibration. Fig. 11 offers an intuitive understanding that the proposed control algorithm for RS-TLCD is only based on output measured signals, no structural modal information and earthquake records are needed, which shows a wide applicability.

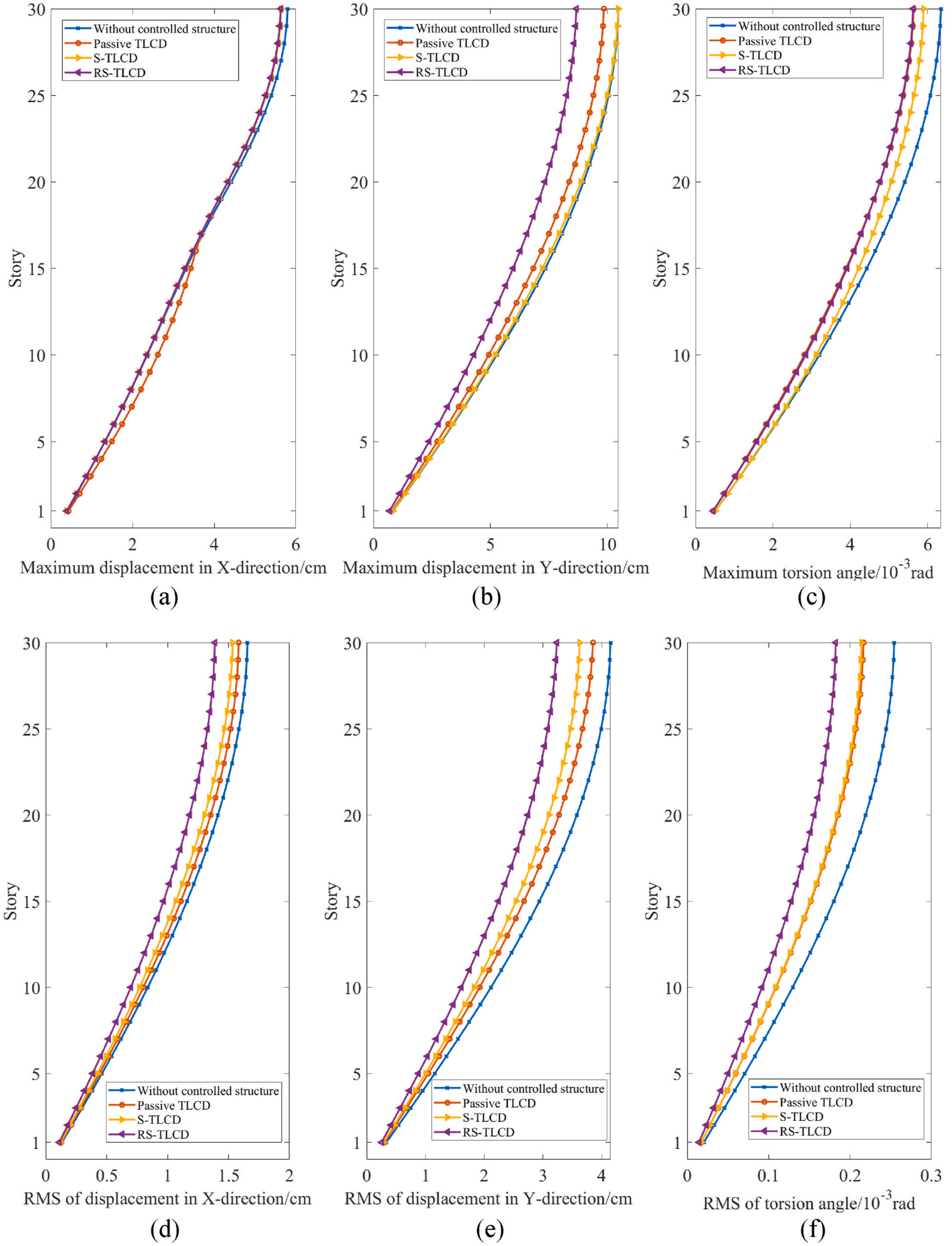

(caption on next page)

Fig. 9. Comparison of structural displacement responses of all stories under the 5th group of bi-directional seismic excitation. (a) Maximum displacement in X-direction; (b) Maximum displacement in Y- direction; (c) Maximum torsion angle; (d) RMS of displacement in X-direction; (e) RMS of displacement in Y- direction; (f) RMS of torsion angle.

Table 8
Structural displacement response reduction with signal noise.

Type	Damper	Maximum of X-displacement	Maximum of Y-displacement	Maximum of torsion angle	RMS of X-displacement	RMS of Y-displacement	RMS of torsion angle
Original	S-TLCD	2.59 %	−0.06 %	7.06 %	7.29 %	12.55 %	15.72 %
Noise		0.02 %	−3.14 %	5.10 %	8.19 %	3.33 %	7.54 %
Original	RS-TLCD	12.66 %	28.04 %	0.59 %	51.24 %	45.16 %	12.90 %
Noise		9.50 %	29.27 %	5.48 %	49.72 %	46.04 %	8.57 %

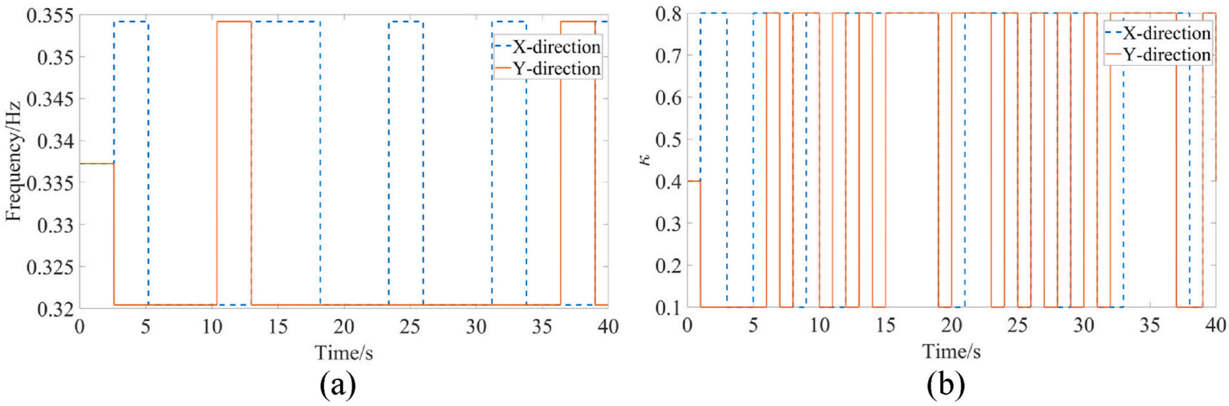

Fig. 10. Instantaneous parameters of two unidirectional S-TLCDs respectively under the 5th seismic excitation. (a) The instantaneous frequency; (b) The instantaneous orifice ratio.

5. Conclusions

To enhance the intelligent disaster mitigation capability of traditional passive TLCD for bi-directionally eccentric structures with coupled translational-torsional vibration under seismic excitations, a novel rotating semi-active tuned liquid column damper (RS-TLCD) with variable hydrostatic liquid level height and frequency, variable orifice ratio and damping, variable rotating angle is proposed in this study. RS-TLCD utilizes an integrated electromechanical system for liquid damping, featuring real-time adjustment of the U-shaped tube liquid column height via water pumps and electromagnetic valve to achieve variable frequency. Additionally, it incorporates variable damping by altering the size of the orifice and introduces a rotatable base at its bottom, enabling angle adjustment to align with the dominant vibration direction of structure and thereby maximizing the control force efficiency.

The variable frequency algorithm comprehensively of RS-TLCD considers the responses in both X and Y directions to determine an ideal tuning frequency which can balance bi-directional vibration states. The variable damping algorithm considers the relationship among the X and Y directional velocity and acceleration responses of main structure, as well as the velocity of RS-TLCD itself, to facilitate bi-directional damping adjustment in real time. Furthermore, the variable angle algorithm balances instantaneous optimal parameters bi-directionally to achieve the best vibration control angle, resulting in superior bi-directional intelligent control performance.

To validate the intelligent control effectiveness of RS-TLCD, the case study in this paper adopts a 30-story bi-directionally eccentric frame structure. Fifteen groups of bi-directional seismic waves are selected for numerical simulation. The response of main structure is discussed under four cases: without control, two optimal passive TLCDs separately arranged in X and Y directions, two unidirectional S-TLCDs, and an RS-TLCD. All the four cases are subjected to bi-directional earthquake excitations. Through multiple simulations, conclusions can be drawn as follows:

(1) Due to the influence of structural eccentricity, the vibration response of structure in Y direction is more significant than that in X direction under seismic excitations.
(2) The seismic mitigation performance of TLCD equipped with a semi-active control system is better than that of passive TLCD. Both RS-TLCD and S-TLCDs demonstrate superior control effect compared to passive TLCDs, in terms of maximum and RMS values of X and Y directional displacement, as well as torsion response. Generally, the vibration control outcomes of RS-TLCD and S-TLCDs are comparable in both X and Y directions.

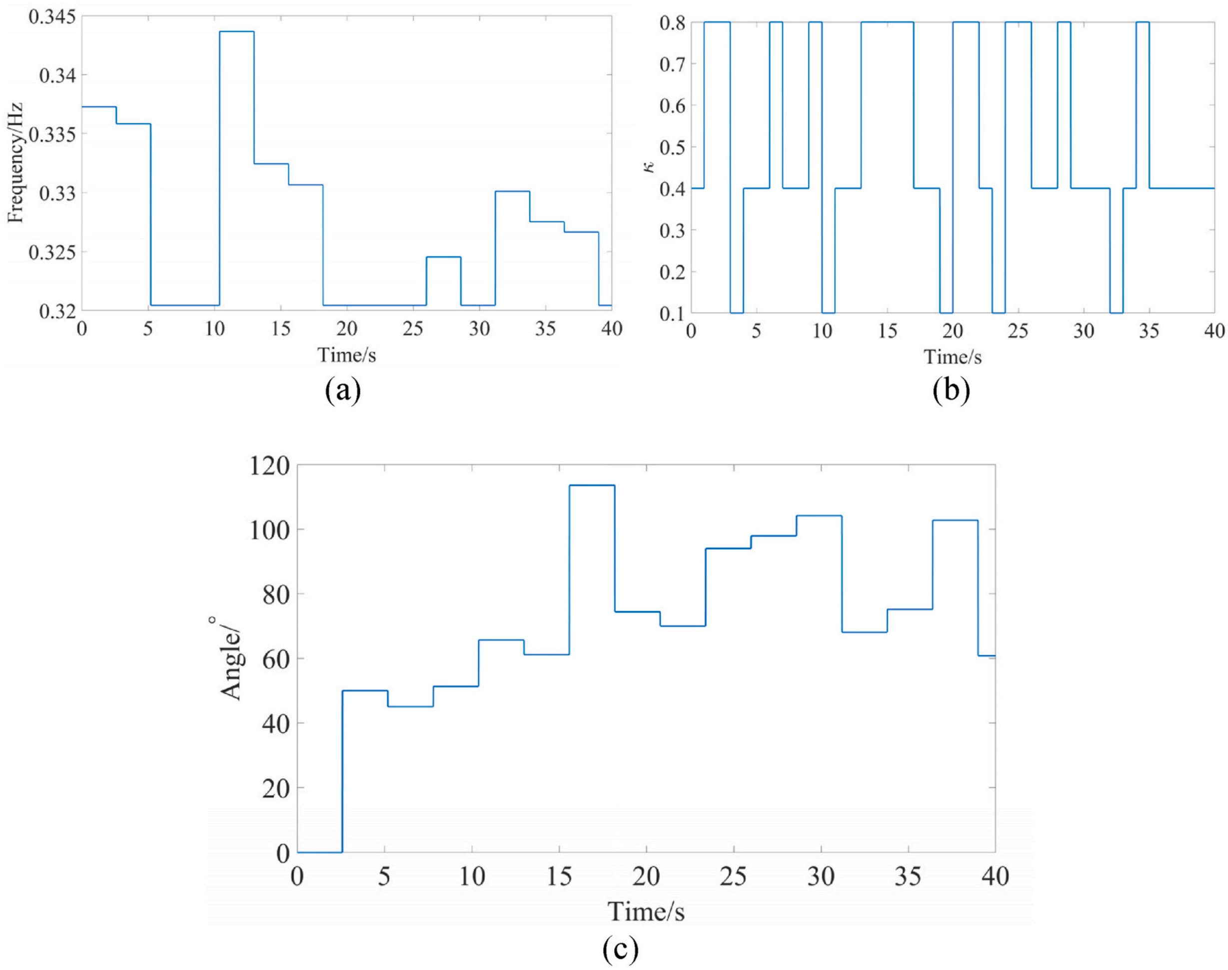

Fig. 11. Instantaneous parameters of RS-TLCD under the 5th seismic excitation. (a) The instantaneous frequency; (b) The instantaneous orifice ratio; (c)The instantaneous angle.

(3) As for torsion response, RS-TLCD exhibits better control performance than S-TLCDs in terms of maximum and RMS values of torsion angle overall. This advantage is attributed to the rotatable base of RS-TLCD, which enables real-time adjustment to the dominant vibration angle and maximizes the control force efficiency.
(4) The RS-TLCD which requires less space within structural space, can remain or even exceed control performance for bi-directional translational and torsional earthquake mitigation compared to two unidirectional passive TLCDs and S-TLCDs.

CRediT authorship contribution statement

Cong Fu: Writing – original draft, Software, Methodology. **Liangkun Wang:** Writing – review & editing, Supervision, Funding acquisition, Conceptualization. **Zhipeng Wang:** Writing – review & editing, Funding acquisition. **Songtao Xue:** Writing – review & editing, Supervision. **Liyu Xie:** Writing – review & editing, Supervision.

Declaration of competing interest

All authors state that there is no conflict of interest.

Acknowledgements

The authors are grateful for the financial support received from the National Natural Science Foundation of China (Grant no. 52308526), the Fundamental Research Funds for the Central Universities (0200121005/174), and the Scientific Research Fund of Institute of Engineering Mechanics, China Earthquake Administration (Grant No. 2023D02).

Data availability

Data will be made available on request.

References

[1] H. Wang, H. Gao, J. Li, et al., Optimum design and performance evaluation of the tuned inerter-negative-stiffness damper for seismic protection of single-degree-of-freedom structures, Int. J. Mech. Sci. 212 (2021) 106805.
[2] H. Gao, C. Xing, H. Wang, et al., Performance improvement and demand-oriented optimum design of the tuned negative stiffness inerter damper for base-isolated structures, J. Build. Eng. 63 (2023) 105488.
[3] S. Colwell, B. Basu, Experimental and theoretical investigations of equivalent viscous damping of structures with TLCD for different fluids, J. Struct. Eng. 134 (1) (2008) 154–163.
[4] X. Zeng, Y. Yu, L. Zhang, et al., A new energy-absorbing device for motion suppression in deep-seafloating platforms, Energies 8 (1) (2014) 111–132.
[5] B. Park, Y. Lee, M. Park, et al., Vibration control of a structure by a tuned liquid column damper with embossments, Eng. Struct. 168 (2018) 290–299.
[6] K.W. Min, J. Kim, Y.W. Kim, Design and test of tuned liquid mass dampers for attenuation of the wind responses of a full scale building, Smart Mater. Struct. 23 (4) (2014) 045020.
[7] Y. Zhou, L. Qian, W. Bai, Sloshing dynamics of a tuned liquid multi-column damper for semi-submersible floating offshore wind turbines, Ocean. Eng. 269 (2023) 113484.
[8] K.A. Al-Saif, K.A. Aldakkan, M.A. Foda, Modified liquid column damper for vibration control of structures, Int. J. Mech. Sci. 53 (7) (2011) 505–512.
[9] M. Tanveer, M. Usman, I.U. Khan, et al., Material optimization of tuned liquid column ball damper (TLCBD) for the vibration control of multi-storey structure using various liquid and ball densities, J. Build. Eng. 32 (2020) 101742.
[10] M.U. Shah, M. Usman, S.H. Farooq, et al., Effect of tuned spring on vibration control performance of modified liquid column ball damper, Appl. Sci. 12 (1) (2021) 318.
[11] B.J. Park, Y.J. Lee, M.J. Park, et al., Vibration control of a structure by a tuned liquid column damper with embossments, Eng. Struct. 168 (2018) 290–299.
[12] Y. Liu, K. Liu, L. Liu, et al., Theoretical and experimental investigation of flexible air spring stiffness in a tuned liquid column gas damper for vertical vibration control, J. Build. Eng. 98 (2024) 110958.
[13] H. Hokmabady, A. Mojtahedi, S. Mohammadyzadeh, et al., Structural control of a fixed offshore structure using a new developed tuned liquid column ball gas damper (TLCBGD), Ocean. Eng. 192 (2019) 106551.
[14] H. Hokmabady, S. Mohammadyzadeh, A. Mojtahedi, Suppressing structural vibration of a jacket-type platform employing a novel magneto-rheological tuned liquid column gas damper (MR-TLCGD), Ocean. Eng. 180 (2019) 60–70.
[15] W. Yu, F. Lemmer, P.W. Cheng, Modeling and validation of a tuned liquid multi-column damper stabilized floating offshore wind turbine coupled system, Ocean. Eng. 280 (2023) 114442.
[16] M.A. Xue, X. Hu, Y.A. Hu, et al., Experimental and numerical study on dynamic response of a photovoltaic support structural platform with a U-shaped tuned liquid column damper, Ocean. Eng. 311 (2024) 118908.
[17] S. Nagarajaiah, Adaptive passive, semiactive, smart tuned mass dampers: identification and control using empirical mode decomposition, Hilbert transform, and short-term Fourier transform, Struct. Control Health Monit. 16 (7-8) (2009) 800–841.
[18] C. Sun, S. Nagarajaiah, Study on semi-active tuned mass damper with variable damping and stiffness under seismic excitations, Struct. Control Health Monit. 21 (6) (2014) 890–906.
[19] S.K. Yalla, A. Kareem, Semiactive tuned liquid column dampers: experimental study, J. Struct. Eng. 129 (7) (2003) 960–971.
[20] I.M. Soliman, M.J. Tait, A.A. El Damatty, Modeling and analysis of a structure semi-active tuned liquid damper system, Struct. Control Health Monit. 24 (2) (2017) e1865.
[21] O. Altay, F. Nolteernsting, S. Stemmler, et al., Investigations on the performance of a novel semi-active tuned liquid column damper, Procedia Eng. 199 (2017) 1580–1585.
[22] O. Altay, S. Klinkel, A semi-active tuned liquid column damper for lateral vibration control of high-rise structures: theory and experimental verification, Struct. Control Health Monit. 25 (12) (2018) e2270.
[23] M. Zimmer, S. Moritz, O. Altay, et al., Hierarchical model predictive vibration control for high-rise structures using semi-active tuned liquid column damper, Struct. Control Health Monit. 29 (10) (2022) e3034.
[24] E. Sonmez, S. Nagarajaiah, C. Sun, et al., A study on semi-active Tuned Liquid Column Dampers (sTLCDs) for structural response reduction under random excitations, J. Sound Vib. 362 (2016) 1–15.
[25] H. Ding, J. Zhang, J. Song, et al., Event-triggered semi-active TLCD for ground motion-induced vibration control, Smart Mater. Struct. 33 (8) (2024) 085038.
[26] C. Masnata, A. Pirrotta, Optimal control of base-isolated systems with sliding TLCD under stochastic process, Eng. Struct. 318 (2024) 118754.
[27] J. Wang, Y. Ni, J. Ko, et al., Magneto-rheological tuned liquid column dampers (MR-TLCDs) for vibration mitigation of tall buildings: modelling and analysis of open-loop control, Comput. Struct. 83 (25–26) (2005) 2023–2034.
[28] Y. Liu, K. Liu, L. Liu, et al., Theoretical and experimental investigation of flexible air spring stiffness in a tuned liquid column gas damper for vertical vibration control, J. Build. Eng. 98 (2024) 110958.
[29] S.K. Lee, K.W. Min, H.R. Lee, Parameter identification of new bidirectional tuned liquid column and sloshing dampers, J. Sound Vib. 330 (7) (2011) 1312–1327.
[30] L. Rozas, R.L. Boroschek, A. Tamburrino, et al., A bidirectional tuned liquid column damper for reducing the seismic response of buildings, Struct. Control Health Monit. 23 (4) (2016) 621–640.
[31] J. Zhang, H. Ding, J.T. Wang, A semi-active toroidal TLCD for multidirectional vibration reduction of structures, Smart Mater. Struct. 31 (12) (2022) 125006.
[32] B. Mehrkian, O. Altay, Omnidirectional liquid column vibration absorbers for multi-story buildings, J. Build. Eng. 62 (2022) 105306.
[33] H. Ding, J.T. Wang, J. Zhang, Design and performance evaluation of toroidal TLCDs in bidirectional seismic control of structures using a modified dynamic model, Structures 69 (2024) 107261.
[34] C. Fu, Application of torsional tuned liquid column gas damper for plan-asymmetric buildings, Struct. Control Health Monit. 18 (5) (2011) 492–509.
[35] M.J. Hochrainer, P.A. Fotiu, Design of coupled tuned liquid column gas dampers for multi-mode reduction in vibrating structures, Acta Mech. 229 (2018) 911–928.
[36] A.S. Ross, A.A. El Damatty, A.M. El Ansary, Application of tuned liquid dampers in controlling the torsional vibration of high rise buildings, Wind Struct. 21 (5) (2015) 537–564.
[37] D.K. Pandey, S.K. Mishra, Moving orifice circular liquid column damper for controlling torsionally coupled vibration, J. Fluid Struct. 82 (2018) 357–374.
[38] L. Wang, Y. Zhou, W. Shi, Random crowd-induced vibration in footbridge and adaptive control using semi-active TMD including crowd-structure interaction, Eng. Struct. 306 (2024) 117839.
[39] Z. Zhang, B. Basu, S.R.K. Nielsen, Tuned liquid column dampers for mitigation of edgewise vibrations in rotating wind turbine blades, Struct. Control Health Monit. 22 (3) (2015) 500–517.
[40] I.E. Idelchik, M.O. Steinberg, O.G. Martynenko, Handbook of Hydraulic Resistance, Hemisphere publishing corporation, New York, 1986.
[41] L. Wang, S. Nagarajaiah, W. Shi, et al., Study on adaptive-passive eddy current pendulum tuned mass damper for wind-induced vibration control, Struct. Des. Tall Special Build. 29 (15) (2020) e1793.
[42] J. Wang, L. Huo, C. Liu, et al., A new acoustic emission damage localization method using synchrosqueezed wavelet transforms picker and time-order method, Struct. Health Monit. 20 (6) (2021) 2917–2935.

[43] J. Wang, L. Huo, C. Liu, et al., Theoretical and experimental study on homologous acoustic emission signal recognition based on synchrosqueezed wavelet transform coherence, Struct. Control Health Monit. (2023) 6968338.
[44] L. Wang, Y. Zhou, S. Nagarajaiah, et al., Bi-directional semi-active tuned mass damper for torsional asymmetric structural seismic response control, Eng. Struct. 294 (2023) 116744.
[45] F. Ferreira, C. Moutinho, Á. Cunha, et al., Use of semi-active tuned mass dampers to control footbridges subjected to synchronous lateral excitation, J. Sound Vib. 446 (2019) 176–194.
[46] H.N. Li, H. Yang, Semi-active control of eccentric structure under multi-dimensional earthquake using MR damper, Earthq. Eng. Eng. Vib. 24 (3) (2004) 167–174.
[47] J. Wang, H. Li, B. Wang, et al., Development of a two-phased nonlinear mass damper for displacement mitigation in base-isolated structures, Soil Dynam. Earthq. Eng. 123 (2019) 435–448.
[48] Y. Yang, S. Nagarajaiah, Structural damage identification via a combination of blind feature extraction and sparse representation classification, Mech. Syst. Signal Process. 45 (1) (2014) 1–23.